A Comprehensive Experimental Investigation of Hydraulically Supported Robot Assisted Incremental Sheet Forming of Al6061 Sheets

Ravi Prakash Singh[1,2], Santosh Kumar[3], Edward J Brambley[1,2], Pankaj Kumar Singh[3], and GM Karthik[3]

[1]Mathematics Institute, University of Warwick, Coventry, CV4 7AL, UK
[2]WMG, University of Warwick, Coventry CV4 7AL, UK
[3]Department of Mechanical Engineering, IIT (BHU), Varanasi U.P.-221005, India

1st October 2024

Abstract

In the current study, robot assisted incremental sheet forming (RAISF) was performed on sheets of aluminum alloy 6061, which was supported from underneath by fluid; this process is named robot assisted incremental sheet hydroforming (RAISHF). A variable wall angle conical frustum was fabricated both with and without the fluid support. The cone formed by RAISHF was 6.67% steeper and 28.47% deeper than with RAISF alone. Spring back was also reduced by 77.14%, suggesting better accuracy of the formed part. For cones of identical wall angle formed with RAISF and RAISHF, the thickness distribution, tensile properties, microhardness, major and minor strains in the plane of the sheet, microstructures, and residual stresses are characterized, with RAISHF showing greater and more even thickness distribution, more even strain distribution, and less hardening. X-Ray diffraction analysis revealed the residual stress in both processes to be tensile, with RAISHF showing lower residual stress. Microstructures of the samples taken from formed cones revealed that, due to dynamic recrystallization, more strain can be obtained by RAISHF.

Keywords: Incremental forming; Hydroforming; Straight groove test; Nakajima test; Forming limit, XRD, Microhardness

1 Introduction

Incremental sheet forming (ISF) does not involve use of dedicated dies for sheet forming and is used for small batch production of complex three-dimension shapes [1]. ISF has been an area of interest amongst researchers and industry alike because of its various advantages over the conventional stamping process, discussed below. Due to the die less nature of the process, it is cost effective for small batches.ISF offers a high degree of shape flexibility, especially for small batch production of complex 3D shapes, and high energy efficiency [2, 3].Emmens and van den Boogaard [3], Gatea et al. [4] explained how strains in ISF can be attained well above the forming limit curve (FLC) for conventional processes like deep drawing, stretching, and stamping. The enhancement of formability is due to localized deformation, resulting in a high level of localized compressive stress between the tool and the workpiece, which squeezes voids and slows down the process of damage, thereby, suppressing/ delaying necking.They further explained the enhanced formability as as a consequence of complex stresses arising during ISF. Factors such as contact stress, bending under tension, shear, cyclic straining, the geometrical inability of the neck to grow, and hydrostatic stress, have been reported responsible for improved formability. Several work has been reported on studying formability in ISF process by means of Straight groove test and Variable Wall Angle Conical Frustum (VWACF) [5–8].

During the initial development of ISF, the process was carried out on a 5/6-axis CNC machine. However, more recently, industrial robotic arms have been used to perform ISF, and the process is called Robot-Assisted Incremental Sheet Forming (RAISF) or Roboforming [9]. Robotic arms offers verious advantages over CNC machines such as better speed control, higher accuracy, and a larger workspace which can be beneficial while forming large and complicated shapes [10–12].However, in recent times, some other changes have also been made in ISF to enhance the capabilities of the process. Some of these are hot/warm forming using induction heating [13–16] Laser-Assisted In-

cremental sheet forming [17, 18], and ISF with ultrasonic vibrations [19, 20]. One of the major drawbacks of ISF is geometrical inaccuracy of the formed product [21–23]. Hirt et al. [24] presented a comprehensive review of the geometrical inaccuracies occurring during ISF. It was suggested that the geometrical inaccuracies arising in the products formed by ISF is due to plastic deformation outside the contact zone, elastic part deflection in the process, spring back due to release of the regular elastic part of the local deformation and induced residual stresses. As the underside of the sheet is free due to absence of any die and elasticity in the sheet there is a problem of spring back which attenuates the surface finish of the formed product [25–27].Use of a partial die from the back of the sheet has been reported to overcome this issue [28]. Researchers have also reported use of a flexible medium from the back of the sheet. The active medium from the back of the sheet not only provides back support during fabrication of the sheet, but also acts as a flexible die for forming which can lead to enhanced shape accuracy of the formed product. Additionally, the process involving use of flexible medium from the back side of the sheet brings in a pressure which can be beneficial to ISF. It can increase overall formability of sheet due to pressure-induced ductility and changes in stress triaxiality which finally results in uniform strain distribution throughout the deformed sheet.The The reported flexible mediums are pressurized air metallic foam, rubber and static fluid [29, 30]. McLoughlin et al. [31] applied pressurized air from the back of the sheet at 0.0035 bar and observed no significant change in the geometrical accuracy of the formed parts. Khalifa and Thiery [32] used gas as an active medium from back side of the sheet, which acted as a supplementary tool, and under controlled pressure, a concave-convex shape was formed. They also used multistage ISF with preform of height with active medium for forming concave-convex shape [33]. It was reported that preform with 75% of the final height gives significant reduction in undesired bending due to decrease in vertical forces. Similar trends in vertical forces were observed by Zimeng et al. [34] while performing FEA analysis of ISF with isostatic pressing from back. Shang et al. [35, 36] used FEA modelling for ISF with hydraulic support and validated with experiments and found that uniformity in thickness distribution of the formed product was significantly improved. The maximum achievable wall angle was also improved while using hydraulic support. Kumar and Kumar [37] developed Incremental Sheet Hydroforming (ISHF) by introducing hydraulic fluid from the backside of the sheet in ISF, for deforming aluminium sheets. Using FEA modeling with Deform 3D, they observed that ISHF required lower forming forces due to increased material ductility compared to ISF. They further employed multi-stage ISHF to achieve wall angles up to 90° while forming conical frustums [38]. Singh et al. [39] further applied multi-stage ISHF with a six-axis industrial robot, noting improved surface finish and reduced spring back in comparison to single-stage processes. Thus, ISHF can be a more capable process of sheet forming as compared to the conventional ISF. Though, several studies have been carried out on incremental sheet forming and hydromechanical deep drawing, related to wall angle, very limited work has been done characterization of several essential aspects of ISHF. The aim of the current work is to broadly compare the processes of ISF and ISHF performed on six axes of industrial robot.In the present work, RAISF and RAISHF processes have been used to form cones from sheets of aluminium alloy 6061. In the present work, RAISF and RAISHF processes have been used to form cones from sheets of aluminium alloy 6061. Tensile and Erichsen ductility test were conducted to determine mechanical properties of the sheet before forming.3 Experiments were conducted to make conical frustums by RAISF and RAISHF using parameters optimized by straight grove test. The respective outputs of both the processes were compared in terms of formability acheived and strain-strain space, **??** thickness distribution, Accuracy of formed product, 4.2, strength and microhardness of the formed products4.3, residual stresses 4.4, and microstructures 4.5.

2 Experimental setup and robotic tool path planning

The experimental setup of robot-assisted incremental sheet forming (RAISF) and robot-assisted incremental sheet hydroforming (RAISHF) as shown in figure 1 was established from scratch in the Production lab facility at IIT (BHU) and was patented with Title of Invention “Robot Assisted High Speed Incremental Sheet Hydroforming Machine” [40]. The setup used in the current work and its working has been described comprehensively in the previous works undertaken by the authors [15, 41, 42]. The experimental set up consists of the main parts which are: a six-axis industrial robot with a payload of 180 kN with a controller and teach pendant, provided by M/s Yaskawa, clamping arrangement, forming tool, tool dynamometer for force measurement fluid chamber (only used for RAISHF),Piston and cylinder assembly to maintain hydraulic pressure, Control Valves (V_1, V_2, V_3) and Pressure sensors and gauge for pressure monitoring. The various parts of the setup has been shown in 1. To avoid any air and fluid leakage from the

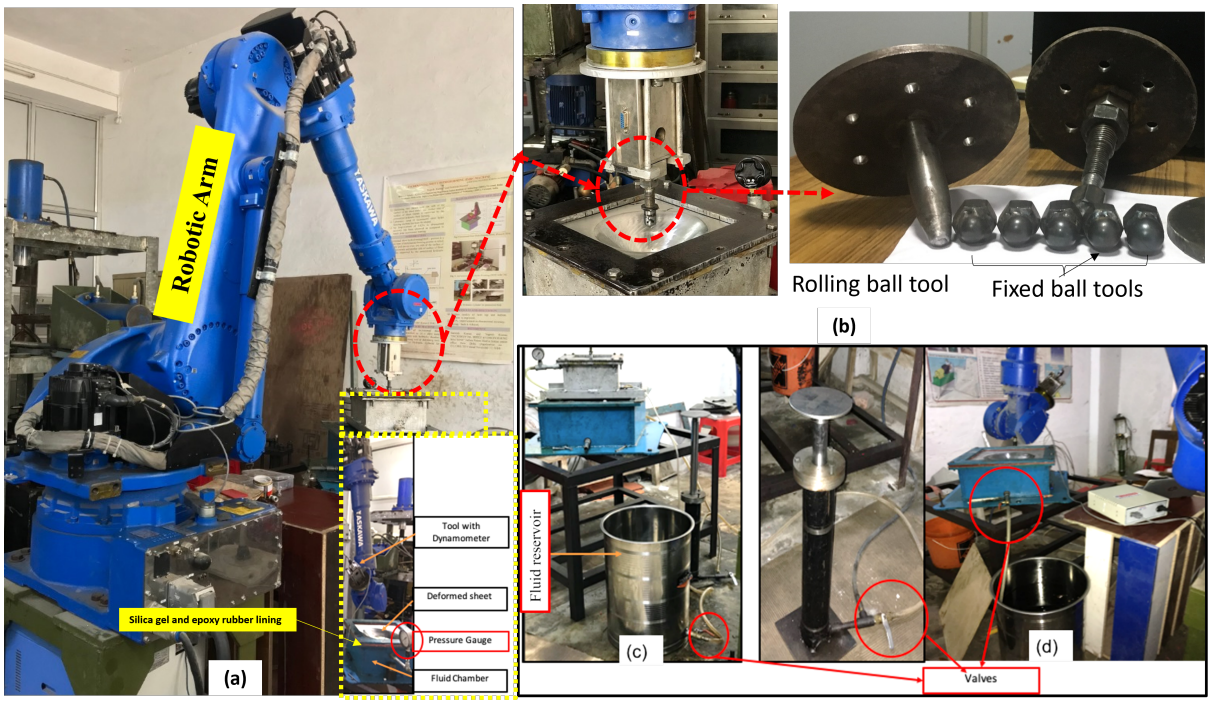

Figure 1: Robot assisted incremental sheet hydroforming setup: (a) CAD model, (b) labelled diagram of existing setup, (c) fluid reservoir, (d) piston and valve arrangement.

fluid chamber, silica gel and epoxy rubber was used between the flange and the fluid chamber. The working methodology of the RAISHF can be understood from figure 2 (a). The fluid chamber was made oil full before thw start of forming. The sheet was clamped between the flanges and was sealed with silica gel and epoxy rubber to make it leak free and airtight. Valves V_1 and V_2 were closed and V_3 was open. Fluid pressure from the back of the sheet is maintained by using piston-cylinder arrangement with a counter weight. It was found that a high pressure (> 1.3 bar), caused bulge in the sheet in the upward direction, and subsequent forming by the tool in the downward direction caused folds in the sheet and crack in the region as shown in the figure 2 (c). Hence a pressure in the range of $1.0 - 1.3$ bar was chosen. This pressure was maintained easily by piston-cylinder arrangement, and naturally is not sufficient for causing any significant plastic deformation, but to act as a support from the back of the sheet to ensure better geometrical accuracy of the formed product and also ensure uniform strain distribution. Similar recommendations have been given by Shang et al. [35, 36]. The cone formed and the pressure generated during the formation of the cone has been shown in figure 2 (b) and (c) respectively. Once the forming was complete Valve V_1 was opened to put fluid back to the reservoir. For tool path planning, couple of methods were adopted.

1. ***Teach pendant based tool path planning:*** In this method, in situ tool path planning was carried out with a teach pendant. This planning was adopted for both axis-symmetric and non-axis-symmetric shapes with fixed wall angles. The process is explained further through a sample program that generates an axis-symmetric cone, as shown in figure 3(a). The process is fast and works efficiently particularly for simple geometries with fixed wall angles.

2. ***Software based tool path planning:*** However, in scenarios involving more intricate shapes, such as those with varying wall angles, the use of the teach pendant for tool path planning becomes less practical as number of points to be specified becomes impractically high. In such instances, a software-based tool path planning strategy is implemented. In this strategy shapes and corresponding tool paths, once generated on 3D modelling software (CATIAV5 in current study) is converted into.stl file to get the information of every layer separated by vertical step depth (). NC file is obtained from .stl file which can be directly fed into the RobotDK software which serves as an intermediary, establishing a seamless interface between the robotic system and computer-based planning. The process for software strategy is shown in Figure 2 (d).

Once the tool path was developed successfully us-

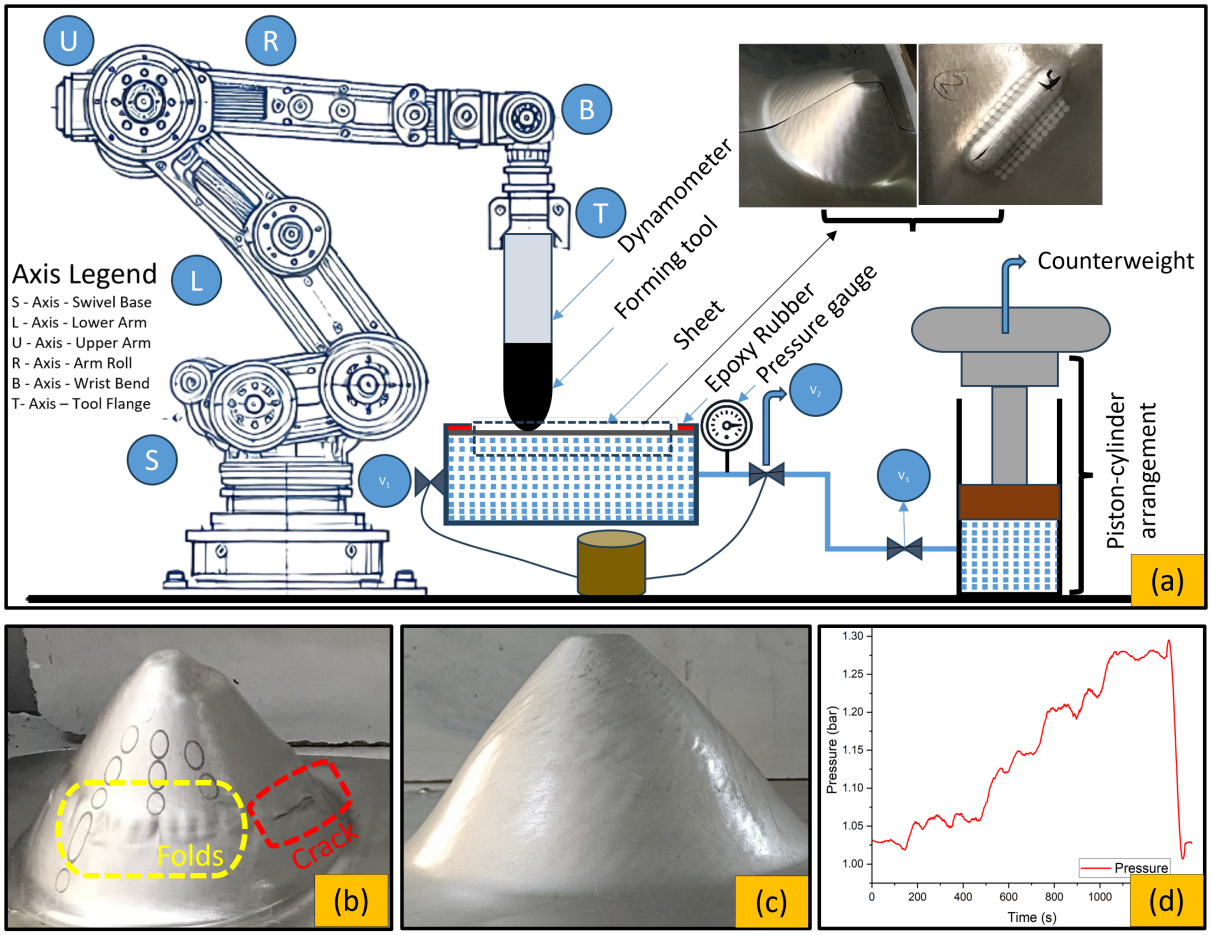

Figure 2: (a)Schematic diagram for working of RAISHF (b) Crack and fold in the sample when formed with a high back pressure (c) successfully foemd cone and (d) Pressure from back during successful formation of cone

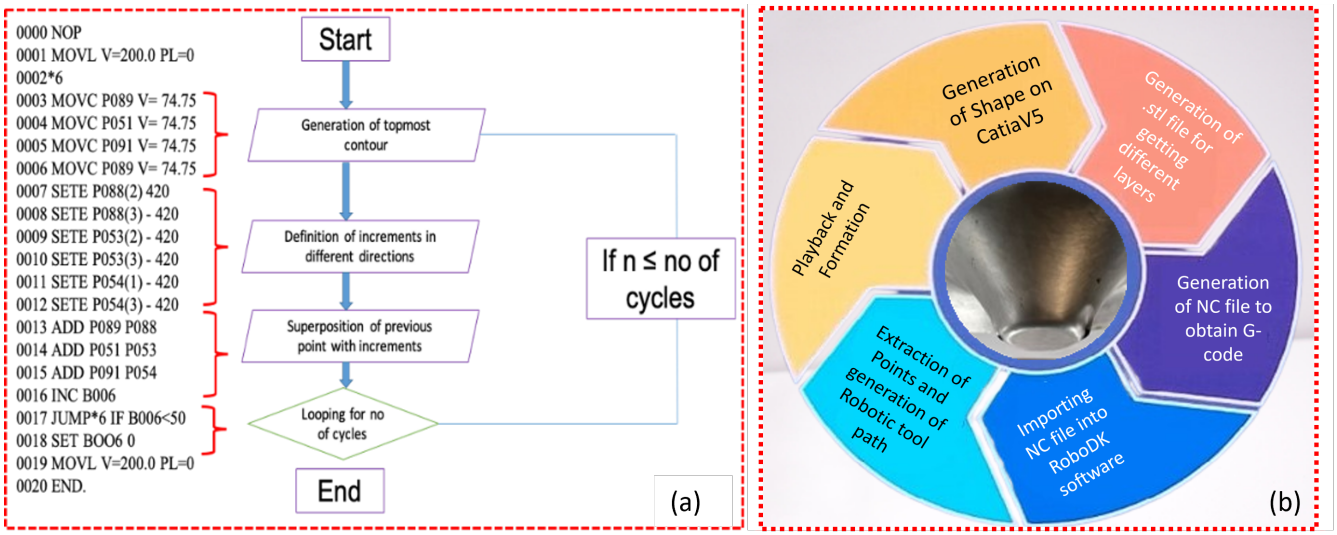

Figure 3: (a) Sample tool path program on teach pendant (c) software-based tool path strategy for VWACF

ing any of the above mentioned two methods, it was tested conducting a dry run of the tool. If the tool motion was accurate, as per the programmed path, the tool was allowed to playback the programmed tool path to fabricate the sheet. The fixed ball tool was used in the current study, as it gives rise to a kinetic friction condition, leading to more localized heating which can induce softening effect to the sheet and hence more deformation can be achieved. The experimental parameters of tool speed, tool diameter, and step depth were selected using straight groove test due to its simplicity and rapid execution. The outputs of depth of groove, spring back and forming time were used for regression analysis to determine the optimal combination of input parameters using the central composite response surface design (CCRSD) on Minitab software. Tool speed and step depth were taken as continuous variables, while tool diameter was categorical. A total of 39 experiments were conducted, and the results optimized for minimizing forming time and spring back while maximizing theoretical depth. The optimum parameter values were tool speed at 85 mm/s, step size at 0.4 mm, and tool diameter at 12.5 mm, achieving a composite desirability of 0.7652 [43]. These optimized parameters effectively balanced the trade-offs between the output responses and were selected for further experiments.

3 Base Material

For this work, sheets of aluminium alloy AA6061 of 1.48 mm thickness were used,; this grade of alumunium is widely used in sheet metal industries. The alloy AA6061 was solution heat-treated for 2 hours at $415°C$ to acheive the homogenized phases and then furnace-cooled to $260°C$ and held for one hour, and finally air cooled [44]. The composition of the AA6061 was determined by optical emission spectrometer and is presented in Table 1. To asses the mechanical properties of the sheet material before forming, tensile test, Erichsen ductility test and Nakajima test was performed.The uniaxial tensile test was performed on a 100 kN INSTRON (MODEL 8801) using samples as per the ASTM/E8 standard. For studying the formability of the AA6061 sheet after heat treatment, Erichsen ductility test was conducted. The specimens were prepared as per the $ASTM/E643/15$ standard. The diameter of indenter was 20mm with main scale division 1 mm, and the circular scale division of $50/5MSD$. Three domes were formed by the indenter utill the onset of fracture of the dome, and the depth of the indentation was measured as (H_D). The tensile properties and the details of the depth of indentation (H_D) of all the domes on the samples of AA6061 preform is presented in Table 2.

The formability of preform material after heat treatment, was evaluated comprehensively in terms of the forming limit curve (FLC). The FLC was measured according to the ISO 12004-2: 2008 standard [45] using the Nakajima test. During the test, a hemispherical punch with a diameter of 100 mm was used to perform out-of-plane stretching on a series of sample geometries, to generate different strain paths, as shown in figure 4 on an ITC Interlaken 1000 kN hydraulic press, equipped with a Nakajima punch and smooth clamp ring set [46].

The sample in Figure 1(a) generates an equibiaxial strain path, while the sample in Figure 1(g) generates a uniaxial strain path. The samples in between produce other strain paths, ranging between these two extremes, including biaxial and plane strain paths. Figure 1(h) shows the orientation of the specimen geometries during the tests. The tests were conducted at a constant punch speed of 1 mm/s. A minimum of three repeats were carried out for each sample geometry. Friction was minimized on the punch by applying a lubrication stack (tallow/Teflon/tallow/PVC/tallow/Teflon/tallow layers) between the specimen and the punch. The failure strain was measured with a GOM 5M digital image correlation (DIC) system using a position-dependent method. The DIC system consisted of two 5MP cameras fitted with 50 mm lenses to capture images of the sample surface at a frame rate of 20 frames per second. A speckled paint pattern was applied to the sample surface before the test, and GOM ARAMIS version 6.1 software was used to acquire and process the captured images to calculate strain [47] [48]. The calculated failure strain values were plotted on the forming limit diagram (FLD) to represent the FLC of the material, as shown in figure5.

4 Results and discussions

Various shapes were made on the existing setup by RAISF and RAISHF, as shown in Figure 6. Once, different shapes had been fabricated successfully, several tests were conducted to compare the two processes.

4.1 Maximum formable angle and Forming limit of RAISF and RAISHF

In RAISF and RAISHF, the formability limit is decided by the maximum wall angle which can be formed before fracture.To find the maximum formable angle, a variable wall angle conical frustum (VWACF) as suggested by Hussain et al. [49] was fabricated. The genetrix of VWACF is shown in

Elements	Al	Ti	Si	Mg	Fe	Mn	Zn	Cr	Cu
Composition (wt.%)	97.35	0.05	0.510	0.95	0.41	0.02	0.06	0.15	0.490

Table 1: Composition of the aluminium alloy AA6061

Tensile Properties		**Erichisen ductile properties**			
Properties	Values		Dome 1	Dome 2	Dome 3
Yield Strength(MPa)	249 ± 0.5	IE	9.34	9.12	8.92
UTS (MPa)	265 ± 0.5	Dome height (H_D)	9.02	8.82	8.61
Elongation(%)	14.50 + 0.1	Average H_D		9.13	

Table 2: Tensile and Erichsen ductility property of AA6061

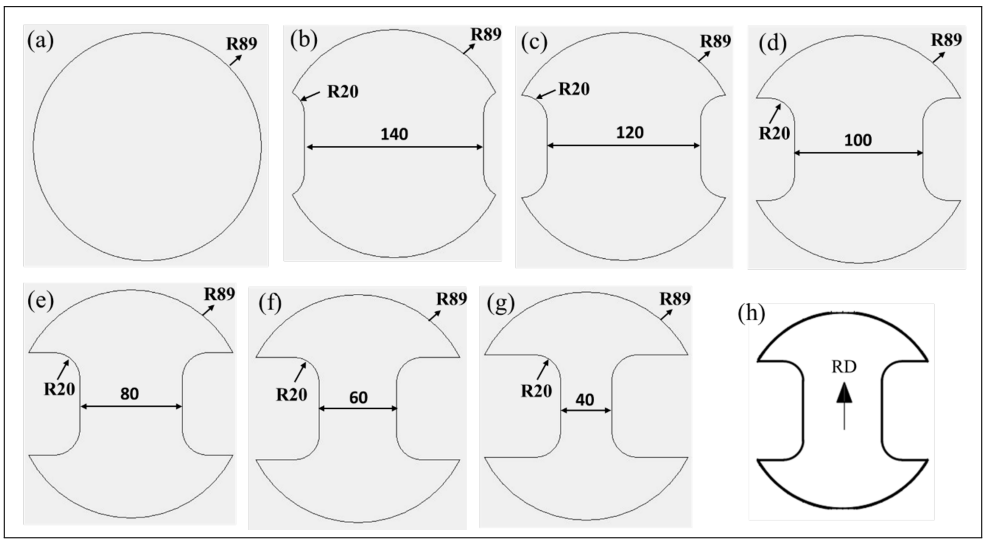

Figure 4: (a-g) Specimens geometries for the generation of FLC and (h) preferred orientation of specimens used in FLC testing.

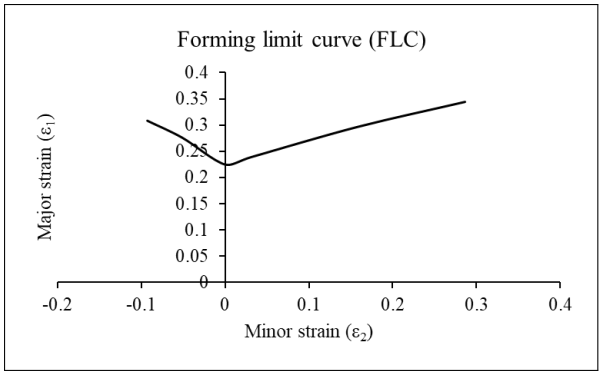

Figure 5: Forming limit curve (FLC) of the base material AA6061

figure 7 (a). The samples made by RAISF and RAISHF are shown in figure 7(b) and figure 7 (c) respectively. The details of the VWACF obtained by RAISF and RAISHF are given in Table 3. It can be seen from Table 3, that larger forming angle and smaller spring back can be achieved by RAISHF compared with RAISF. In case of RAISHF, the forming angle and forming depth increased by 6.67% and 28.47% respectively. As there is a presence of fluid in the back surface of the sheet, this fluid exerts pressure on walls of the cone being formed reducing the stress in the thickness direction (σ_t) which can further decrease the level of mean stress. The stress triaxiality can be impacted, which is given by ratio of the mean stress (σ_m) and equivalent stress (σ_e) [50–52]. Due to this, stress triaxiality decreases preventing voids to grow, postponing the final fracture and causing an apparent enhancement formability [53–55].Additionally the fluid from back can also lead to enhanced ductility due to delay in onset of void growth [56–58]. Once the maximum wall angle was predicted using VWACF test, fixed angle conical frustums were successfully fabricated by RAISF and RAISHF under the experimental condition, as optimized after straight groove testing. The initial radius of the cone circle has been taken as 100 mm. The maximum wall angles of the cones formed from sheets were found to be 60° with RAISF and 64° with RAISHF.The improved formability was further demonstrated by comparing strain in the plane of the formed cones of fixed wall angle of 60° fabricated by both RAISF and RAISHF. The undeformed sheets were engraved with circular grid pattern, and these became elliptical when fabricated into conical shapes. Both the cones have been engraved with circular grid patterns. The grid making method recommended by Keeler [59] has been used for engraving different regions of the sheet using a 50 W Fibre laser. Various grid patterns and methodology of grid marking has been discussed by Ozturk et al. [60].The diameter of the engraved circular pattern is 10mm. After deformation, the circular pattern became elliptical. The major and minor axes have been measured, the true major strains and minor strains are calculated using equations 1 and 2.

$$\text{Major strain} = \frac{Major\ axis\ length}{Circle\ diameter} \quad (1)$$

$$\text{Minor strain} = \frac{Minor\ axis\ length}{Circle\ diameter} \quad (2)$$

The scatter plot of major strain vs. minor strain for RAISF and RAISHF is shown in figure 8 which represents forming limit for the two processes. It can be seen from figure 8 (b), that more safe strain can be obtained in case of RAISHF than in RAISF. As discussed above the state of stress triaxiality can lead to void suppression leading to delay in onset of necking. Additionally, of fluid from the back side of sheet acting as a hydraulic support can give rise to some hydrostatic pressure which contributes towards pressure induced ductility to sheets [56, 57, 61, 62]. Hence, the sheet with fluid underneath can be more ductile and larger formability can be achieved by RAISHF than by RAISF.

4.2 Thickness distribution and Accuracy of formed product

As RAISHF is incorporated by presence of hydraulic support from back of the sheet, this support helps in increasing the accuracy of the formed part. The cones fabricated by RAISF and RAISHF have been used for comparison of mechanical properties of the cones formed by RAISF and RAISHF. For evaluating the thickness distribution and the accuracy of the formed product, the cone was cut precisely into two halves with wire electro-discharge machining (W-EDM) and the conical region was divided into 7 sub-regions (0-6), as shown in figure 9(a). The thickness in the different regions has been measured by micrometre with conical tips and least count of 0.001 mm. Region-0 is the undeformed region where thickness is 1.48 mm. The measurement was taken 4 times and average of all four readings has been reported. The thickness plots for the RAISF and RAISHF processes are shown in 9(b).

It was found that there was a certain amount of thinning of the sheet associated with the process of RAISF as well as RAISHF. The sheet is found to be thinnest in the region 1-2 which is nearly at the start of the conical frustum. The sheet is found to be thinnest in this region because of combined bending and stretching taking place in this region. The thickness of the cone is found to be nearly uniform in the regions 2-5. In these regions, the thickness of the sheet can be approximated by sine law. This trend has been frequently reported by previous researchers Ambrogio et al. [63] and Young and

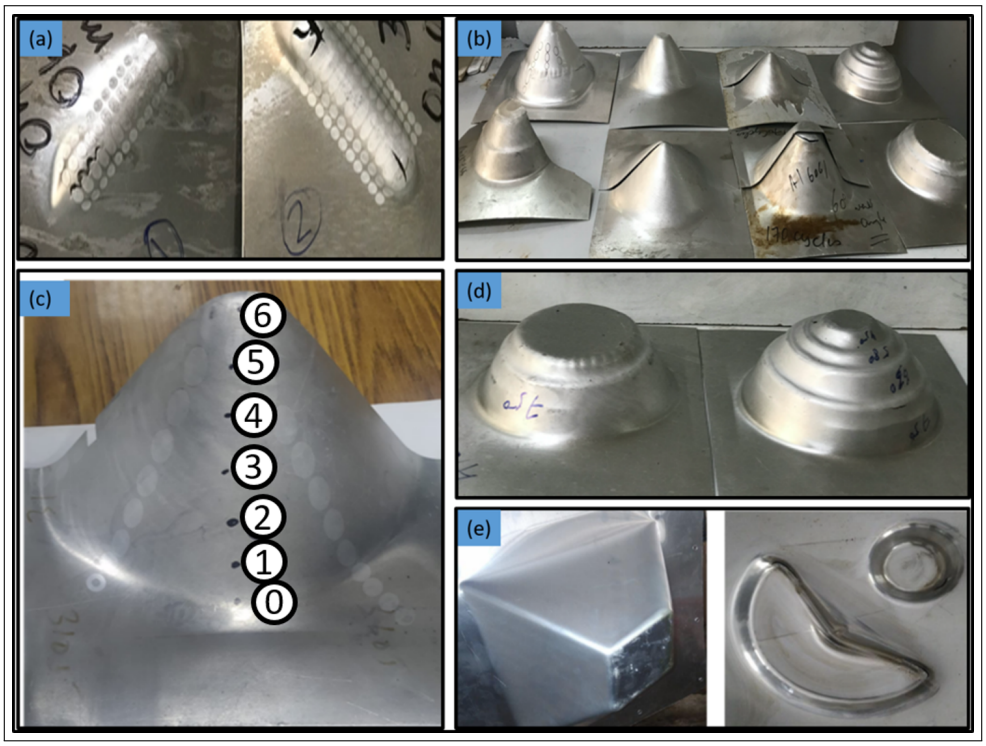

Figure 6: Various shapes fabricated using RAISF and RAISHF: (a) straight groove, (b) conical shape, (c) stepped conical shape, (d) square pyramid, and (e) multi-feature shape

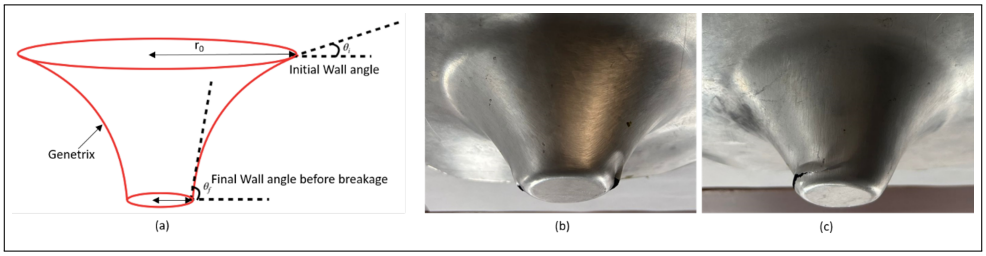

Figure 7: (a) Genetrix of VWACF with initial and final wall angle, (b) VWACF fabricated by RAISF, and (c) VWACF fabricated by RAISHF

Process	Initial Wall angle (°)	Final Wall Angle (°)	Theoretical depth of cone (mm)	Achieved depth of cone (r
RAISF	30	60	36.60	32.42
RAISHF	30	64	42.76	41.65

Table 3: Details of VWACF fabricated by RAISF and RAISHF

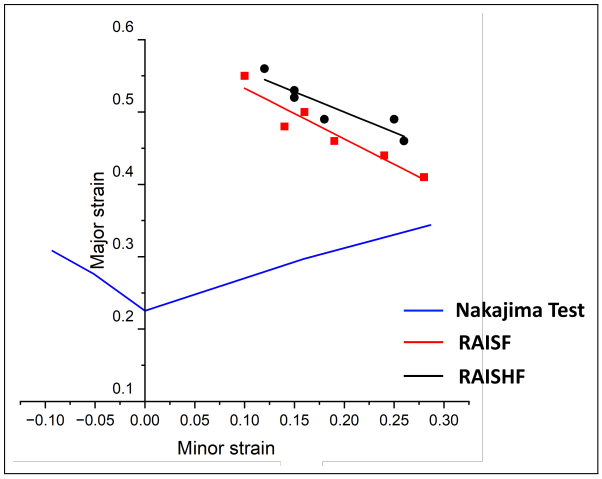

Figure 8: Comparison of forming limit obtained in RAISF and RAISF on Major strain-Minor strain Plot of AA6061

Jeswiet [64], who showed that in middle region of the formed cone, thickness prediction by sine law is most accurate. The blue line in Figure 9(b) shows the thickness, as predicted by the sine law for spinning, $t = t_{\circ} sin(\pi/2 - \theta$ (where θ is the wall angle) [65]. In region 6, which is near the undeformed cone , the thickness again increases. The average sheet thickness t_{avg} in the regions 1-5, is given in Table 4. For RAISHF, thickness in the region 1-5 is more than that in RAISF, hence sheet thinning can be avoided to a significant extent. The average sheet thickness of the cone formed by RAISHF is found to be 12.09% more than that formed by RAISF. As it could be seen in the previous sections that, more in-plane strain can be obtained in case of RAISHF. From volume constancy it can be said that

$$\epsilon_{thickness} + \epsilon_{major} + \epsilon_{minor} = 0 \tag{3}$$

Hence, lesser thickness strain can be seen in RAISHF than RAISF. It can be understood that relatively more uniform strain distribution can be observed in RAISHF also reported by FEA analysis Shang et al. [35, 36]. It has been further observed that in region 1 to region 6 in which extent of deformation is maximum, the range of deviation of thickness values from average value varied from -15.34% to 17.27% in case of RAISF whereas in case of RAISHF the variation lied in the range of -8.84% to 5%. A more uniform thickness distribution can directly make the part more accurate which can be further confirmed by knowing the extent of spring back.

Spring back is basically deviation of wall angle from theoretical wall angle due to presence of elasticity in the sheet material. After the tool leaves the local contact with the sheet, there is an elastic release of deformation due to which spring back occurs. The theoretical wall angle (ϕ_t) can be simply calculated as ratio of increments in vertical and radial direction as shown in figure 10 (a) and (b) and equation 4.

$$\phi_t = tan^{-1}(\frac{\Delta Z}{\Delta r}) \tag{4}$$

Due to natural elasticity present in the sheet, actual wall angle (ϕ_a) is lower than the theoretical wall angle(ϕ_a). The (ϕ_a) was obtained by equation 5

$$\phi_a = tan^{-1}(\frac{H}{R_u - R_L}) \tag{5}$$

Spring back was calculated as percentage difference between theoretical and actual wall angle illustrated by equation 6

$$\text{Spring back}(\%) = \frac{(\phi_t - \phi_a)}{\phi_t} \times 100 \tag{6}$$

The details of cone formed along with springback details have been given in table 5. It can be seen from Table 5 that, the spring back in RAISHF reduced appreciably in comparison with RAISF. A reduction of 73.09% in spring back was recorded while forming cone of 60° wall angle. It can be concluded that strain distribution is much uniform in RAISHF leading to more accurate part with highly reduced spring back due supporting nature of fluid during RAISHF.

4.3 Tensile and microhardness test

To compare tensile properties before and after forming, uniaxial tensile tests have been conducted on the samples, on a 100 kN INSTRON (MODEL 8801). The samples have been prepared as per the standard ASTM/E8 [66]. Since there can be anisotropic effect in the formed product, hence the test samples have been prepared in three orientations: namely, (a) along the length of the formed cone (meridional direction) (b) along the direction of the tool motion (circumferential direction) (c) along 45° direction to meridional direction as shown in Figures 11 (a), (b) and (c) respectively. Tensile samples prepared from the various orientations are shown in Figure 11 (d). The engineering stress strain curves for the various tests conducted are shown in Figure 11 and the tensile properties obtained in various directions are presented in Table 6. It is worthwhile to note that tensile test performed on samples taken from deformed cone has pre-strain leading to low elongation exhibited by these samples. It can be seen from Table 6, that tensile properties in different directions are different, showing anisotropy due to tool direction and deformation in the formed cone. The strength of the cone was maximum in the circumferential direction which is in accordance with the analytical model proposed by Silva et al. [67]. Additionally, it

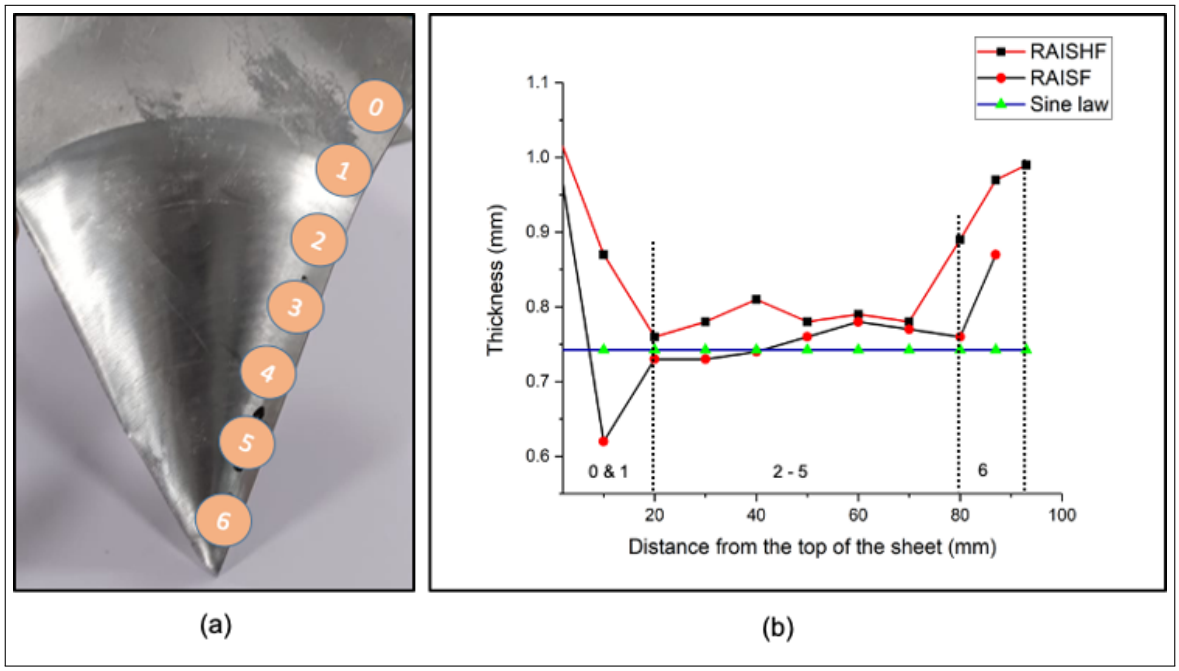

Figure 9: (a) Various regions along the length of the cone where thickness is measured and (b) variation of wall thickness of cones formed by RAISF and RAISHF processes, along the meridional plane.

Process	Average sheet thickness (t_{avg}) (mm)	Minimum thickness (mm)
RAISF	0.736 ±0.001	0.623 ±0.001
RAISHF	0.825 ±0.001	0.752 ±0.001

Table 4: Thickness details of sheet along the length of the cone wall

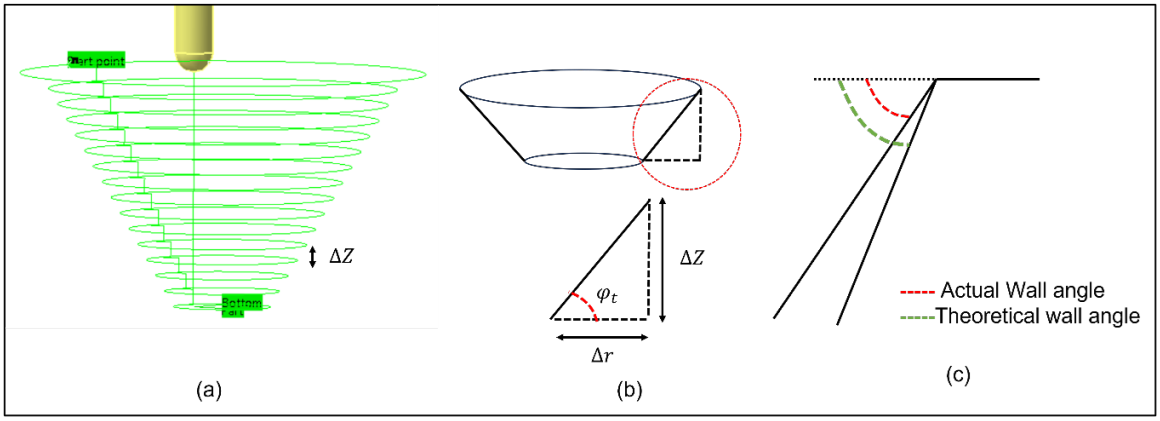

Figure 10: Schematic representation of actual and theoretical wall angles.

Process	θ_t	No. of cycles (N)	θ_a	Spring back (%)
RAISF	60	150	53.37	11.04
RAISHF	60	150	58.21	2.97

Table 5: spring back details of formed cone

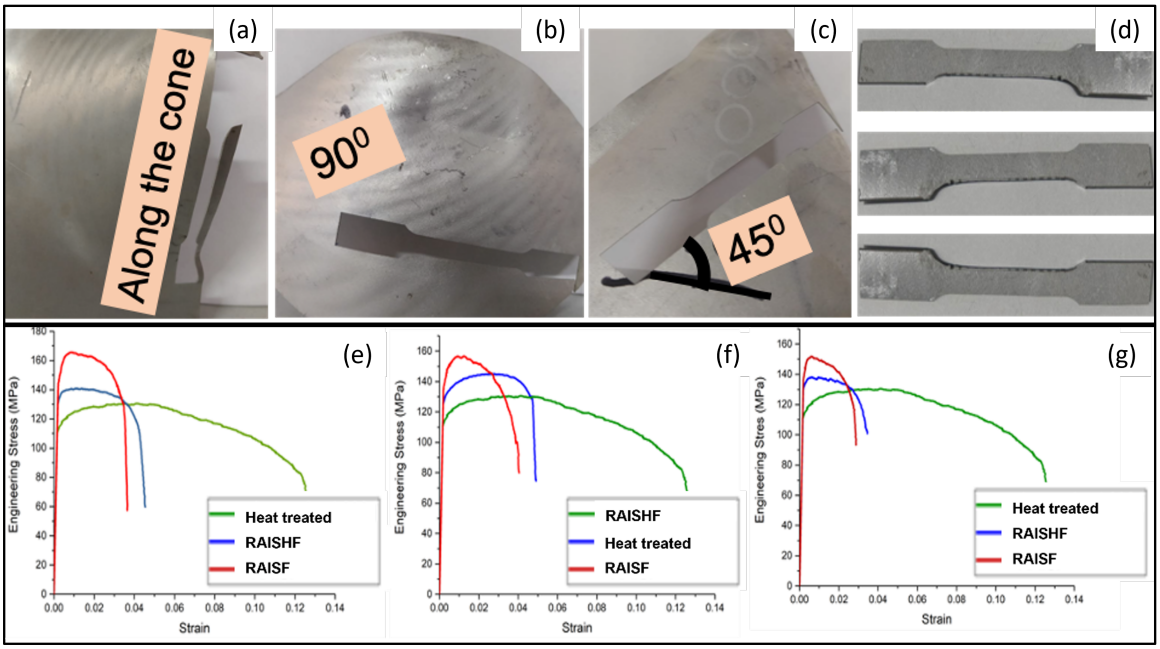

Figure 11: (a)-(c)Tensile samples made in different orientations of the cone (d) various tensile samples. (d)-(f) Stress -strain plot along differnt directions: (d) circumferential direction, (e) meridional direction, and (f) at 45° from the meridional direction.

	Tensile properties along circumferential direction		
Parameters	Heat treated	RAISF	RAISHF
0.2% offset YS (MPa)	112	142	133
UTS (MPa)	127	162	136
Elongation (%)	12.16	3.81	4.14
	Tensile properties along meridional direction		
0.2% offset YS(MPa)	112	130	123
UTS (MPa)	127	157	141
Elongation (%)	12.16	4.12	5.04
	Tensile properties of the cone along 45 degrees		
0.2% offset YS(MPa)	112	145	126
UTS (MPa)	127	146	128
Elongation (%)	12.16	2.54	4.08

Table 6: Tensile properties of the cones formed by RAISF and RAISHF, in different orientations.

Region	RAISF (VHN)	RAISHF (VHN)
0	75.0	75
1	81.6	74.8
2	90.5	70.5
3	90.2	81.2
4	104.2	80.2
5	93.5	98.2
6	83.2	76.0

Table 7: Average microhardness values obtained in different regions of the formed cones.

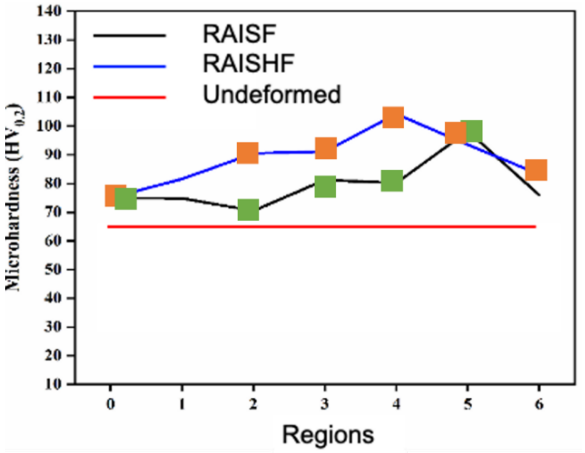

Figure 12: comparison of microhardness of the cones formed by RAISF and RAISHF

can also be seen from the Table 6, that strength of samples taken from the cone formed by RAISHF is relatively less. However, elongation is more in those samples. The reason for relatively lower strength in the case of the hydroformed cone can be stress delocalization due to the static fluid pressure due to hydraulic support from the back. The pressure-induced ductility can account for the rise in ductility of the cone formed by RAISHF .However further studies need to be carried out to find out the quantitative analysis of these effects.

The hardness of the sheet, following RAISF and RAISHF, was examined as it is vital for the fabricated parts to be strong and hard. Testing has been carried out on OMNITECH microhardness testing machine. The applied load was 100 g and indentation time was 10 seconds. For each region, 4 micro measurements have been made at different points on the samples and average of the four values has been taken as microhardness of that region. Average microhardness of undeformed AA6061 sheet is found to be VHN 64. After the cone had been successfully fabricated, samples have been taken from each region (0-6) and microhardness of the different regions has been measured. The respective values of microhardness of the cones of AA6061 formed by the RAISF and RAISHF are recorded in Table 7. As can be seen from Table 7, microhardness values of the samples taken from the RAISF cone are higher in comparison with the samples taken from the respective regions of the cone formed by RAISHF. The microhardness of the samples taken from the formed cones is found to be higher than that of the undeformed sheet, due to strain hardening induced during the process of forming. It may be seen from Figure 12, that microhardness is maximum in middle region of the cone; it suggests that this region has undergone maximum strain hardening due to maximum straining which is also depicted by thickness distribution curve shown in Figure 9. Pressure induced ductility improves the ductility of the sheet which cause strength-ductility trade off [68] decreasing the microhardness of the hydroformed sample. Hence it should be kept in mind, strength gets compromised in RAISHF compared to RAISF.

4.4 Residual Stress

To further access the mechanical properties of the formed product, the residual stress of the samples taken from region 4 of the cone has been measured as this is the region of maximum deformation. Samples have been prepared and $d-sin^2\Psi$ methodology has been adopted for calculation of residual stresses in the samples [69–71]. Three samples have been taken; (a) undeformed sample (b) sample from cone made by RAISF (c) sample from cone made by RAISHF. The definition of specimen frame of reference (FOR), rotated user FOR and different rotation and tilt angles are shown in Figure 13. S_i represents the specimen FOR where S_3 is perpendicular to specimen plane and S_1 and S_2 represent two perpendicular directions in the plane of the specimen. L_i is the user FOR with L_3 perpendicular to the (hkl) plane undergoing diffraction and L_1 and L_2 represent two perpendicular directions in (hkl) plane. In $d - sin^2\Psi$ approach, the strain is calculated by shift in the diffraction peak which gives the change in interplanar spacing. The strain component $\epsilon_{\phi\psi}$ can be written for the rotation angle (ϕ) and tilt angle (ψ) with interplanar spacing determined from the diffraction peak for a certain plane as given by equation 7.

$$\epsilon_{\phi\psi} = \frac{d_{\phi\psi} - d_0}{d_0} \tag{7}$$

Where $d_{\phi\psi}$ is the inter planar spacing at (ϕ, ψ) and d_0 is the interplanar spacing for strain free lattice spacing.The X-ray diffraction gives the value of inter-planar spacing d_0 and $d_{\phi\psi}$. The plot between

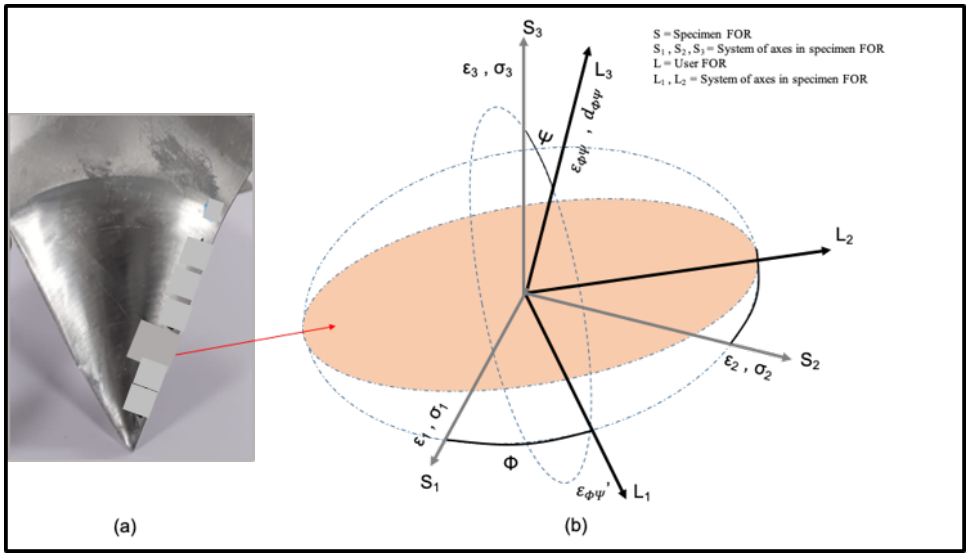

Figure 13: (a) Sample for XRD and (b) definition of different FORs and different angles for XRD examination.

$d_{\phi\psi}$ and $sin^2\psi$ is made by linear fit and measuring the slope and intercept can give the value of stress components. If there is presence of shear components then ψ – splitting occurs. The nature of residual stress in both the samples, taken from the cones formed by RAISF and RAISHF is found to be tensile. Similar results for ISF was obtained using FEA by Kumar et al. [70] Additionally, because of ψ – spilt it can be said that shear stress is also produced during both of the processes. The values of stresses for the undeformed, RAISF and RAISHF samples for $\phi = 0°$, 45° and 90° are given in Table 8. It can be seen from Table 8 that, the nature of residual stress is tensile in the cones formed by both the processes, and tensile residual stress is relatively larger in the cone formed by RAISF.

4.5 Microstructure evolution by EBSD

The study of microstructure and texture evolution has been done by performing Electron Back Scattered Diffraction (EBSD) on Zeiss Gemini, equipped by OXFORD fast CCD detector. For analysis of data obtained from EBSD, the TSL-OIM software has been used. The EBSD scans were taken with a step size of 0.15 μm. Three samples have been tested: (a) undeformed sample (UD) (b) sample taken from region 4 of cone formed by RAISF (c) sample taken from region 4 of cone formed by RAISHF. EBSD data has been used for getting inverse pole Figure (IPF), image quality (IQ) maps, and grain average misorientation (GAM) plot. The IPF plot, IQ map and GAM plot of undeformed samples are given in Figure 14. It may be observed from Figure 14 (a) and (b), that equiaxed fully recrystallized grains are present as the sheet was in fully annealed condition. The average grain size is found to be 8.3 μm. The grains appear to be relaxed due to absence of any strain as annealing caused recrystallization giving rise to stress free grains. Figure 15 gives the plot of number fraction vs. misorientation angle. The misorientation angle greater and less than 15°, are associated with high angle grain boundary (HAGB), and low angle grain boundary (LAGB) respectively. The misorientation angle analysis data shown in Figure 15 (a) shows that high density of high angle grain boundaries (HAGBs) is present in the undeformed sample. It has been further calculated that 26.2% of grains are separated by low angle boundaries and 73.8% of the grains are separated by high angle boundaries. As cone is formed, the sheet gets deformed, due to this deformation, the grains got elongated along the tool motion. The IPF of sample deformed by RAISF and RAISHF are shown in Figure 16 (a) and (c) respectively. It has been observed that grains became refined due to cold work imparted to the sheet. The average size of grains in the samples obtained from the cones formed by RAISF and RAISHF, are found to be 5 μm and 7.1 μm respectively. Refined grains can be seen from the IPFs with different colours for LAGBs and HAGBs shown in Figure 16 (a) and (c). Because high plastic deformation occurred in both the processes, it caused grain fragmentation and led to fine grain evolution. It can be seen from IQ map of RAISF sample, that there are cell blocks present with dense dislocation walls. The cell blocks form at the start of the deformation which activates different slip systems in a grain [72, 73]. It has been observed from IPF of the undeformed sample that

Name of sample	$\phi = 0°$	$\phi =)45°$	$\phi = 90°$
Undeformed	8.4 ± 0.3MPa	43.8 ± 0.3MPa	78.8 ± 0.3MPa
RAISF	52.3 ± 1.1MPa	64.9 ± 1.1MPa	77.5 ± 1.1MPa
RAISHF	45.9 ± 0.4MPa	44.5 ± 0.4MPa	43.0 ± 0.4MPa

Table 8: Values of residual stresses in different samples, at different orientations

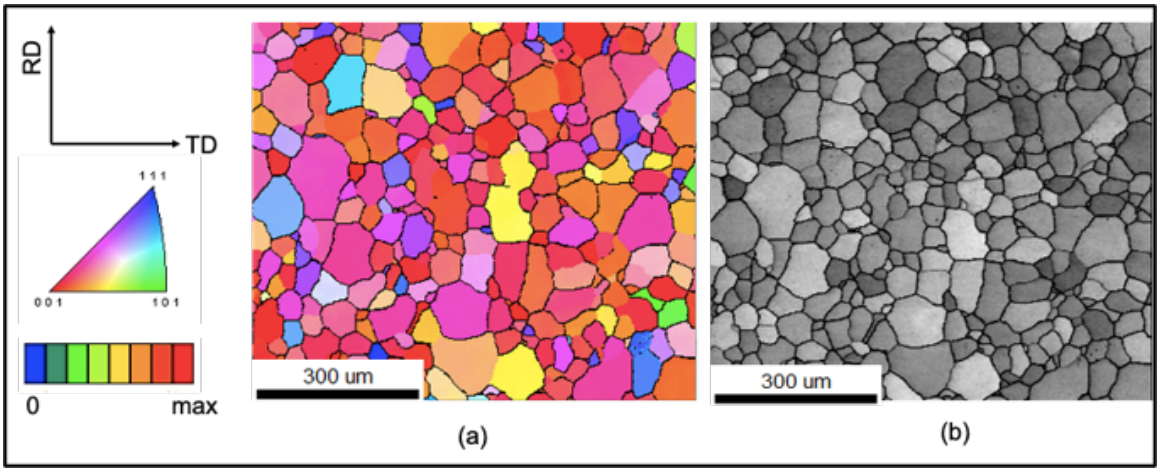

Figure 14: EBSD of undeformed AA6061 in annealed condition (a) IPF plot and (b) IQ map

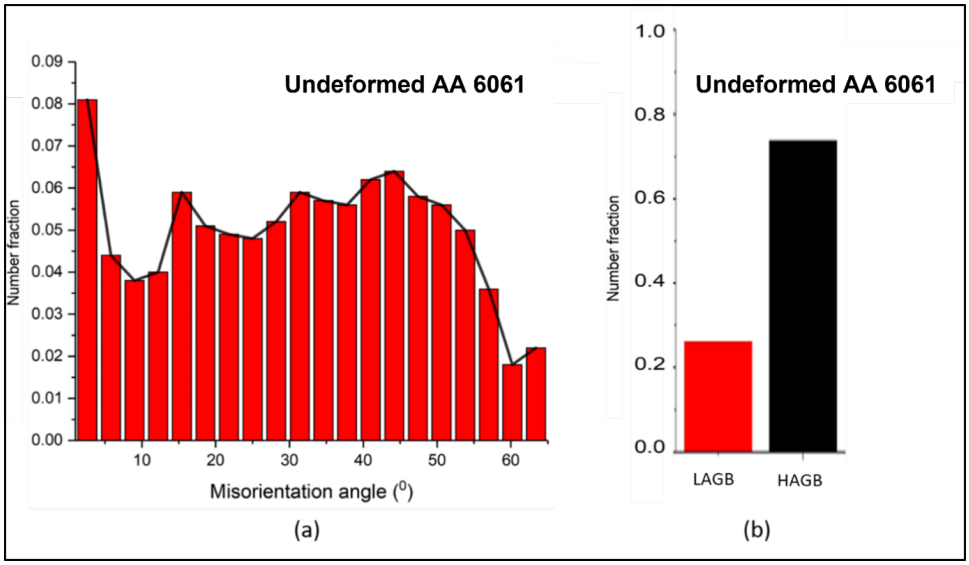

Figure 15: Distribution of misorientation angle in the undeformed AA6061 sample

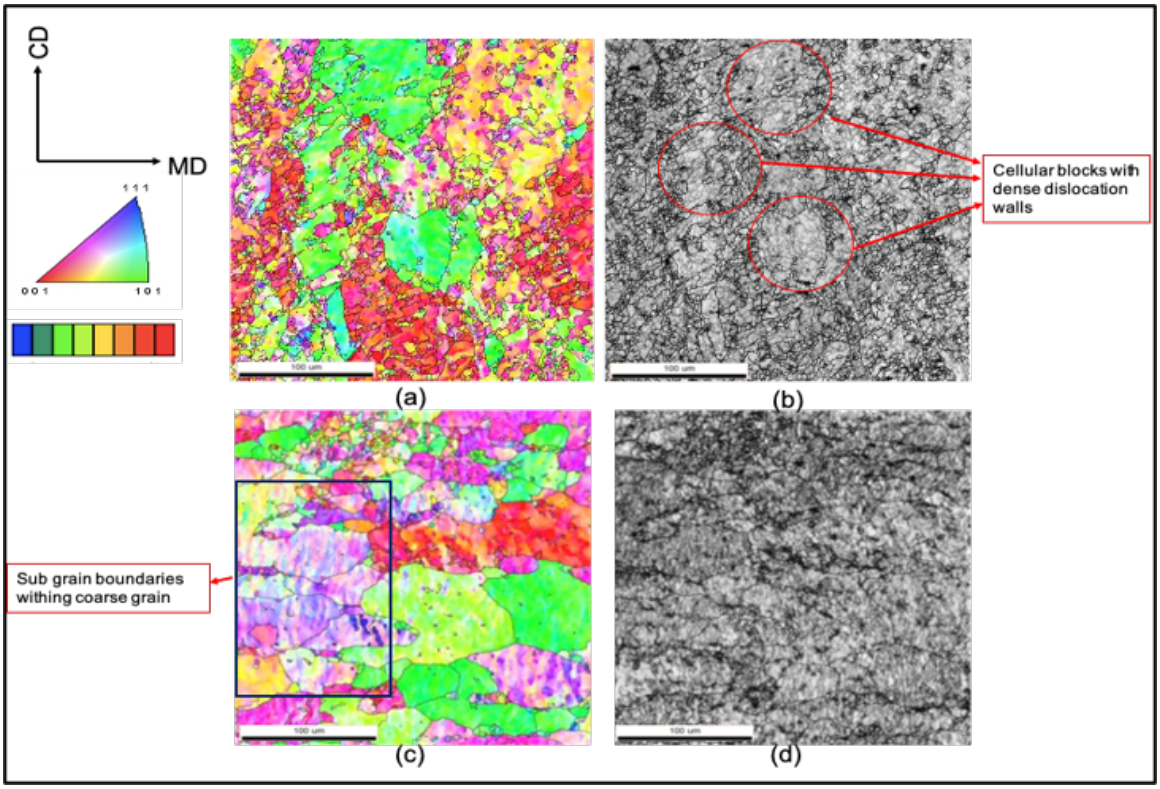

Figure 16: (a) IPF of sample formed by RAISF, (b) IQ map of sample formed by RAISF, (c) IPF of sample formed by RAISHF, and (d) IQ map of sample formed by RAISHF

there were LAGBs present in it. As the sheet gets deformed, these LAGBs act as a site for nucleation of new grains and the formed cellular blocks are surrounded by dense dislocation walls.In case of RAISHF, it was observed that apart from cell blocks with dense dislocation walls, coarse grains are present which contained fine sub grain boundaries which can be observed by colour gradient within the coarse grains in figure 16 c.

Although, in case of both RAISF and RAISHF grain refinement occurred but in case of RAISF finer grains are found to be present. Presence of finer grains in RAISF sample can also be confirmed by the results of tensile test and Hall-Petch according to which, sample with finer grains have higher strength. It has been observed from the tensile test that the strength of the RAISF sample is more than that of the RAISHF sample. A similar result for incremental sheet forming has been observed by Chang et al. [73] and Kumar et al. [74][63] where finer grains were observed in the deformed sample. In case of RAISHF more strain has been obtained, and the result is supported by Kernel misorientation map (KAM). The KAM plot of RAISF and RAISHF samples are shown in Figure 17 (b) and (e) respectively. It can be seen from KAM plot that RAISHF sample has undergone more strain during the process.Further, it can be observed from Figure 17 (a) and (c) that high density of low angle or sub-grain boundaries are present in both the samples. LAGBs are a characteristic of the processes involving cold work [75–77]. Further, in case of RAISF, majority of LAGBs liedlay in the region of 5°–15° whereas in case of RAISHF they are found to be in the region of 1°–5°. During the RAISF process since the material experiences more thinning, it undergoes more through thickness deformation , leading to more dislocations and resulting in dynamic recrystallization of fine grains. Whereas in the case of the RAISHF process, since the samples are thicker than that of the RAISF process, the process of dynamic recrystallization is incomplete. It can be seen from the IPF of RAISHF sample in figure **??**c that there are more sub grain boundaries and higher KAM also reflect higher dislocations in the samples.

5 Conclusion

In the current work, a comparative study of forming of the AA 6061 sheet by two forming processes, RAISF and RAISHF, has been presented. Tensile test and Erichsen ductility test have been performed to evaluate tensile properties and formability of the sheet before deformation. Several shapes have been made using the two processes and their properties have been compared. Experiments have been performed on parameters obtained from

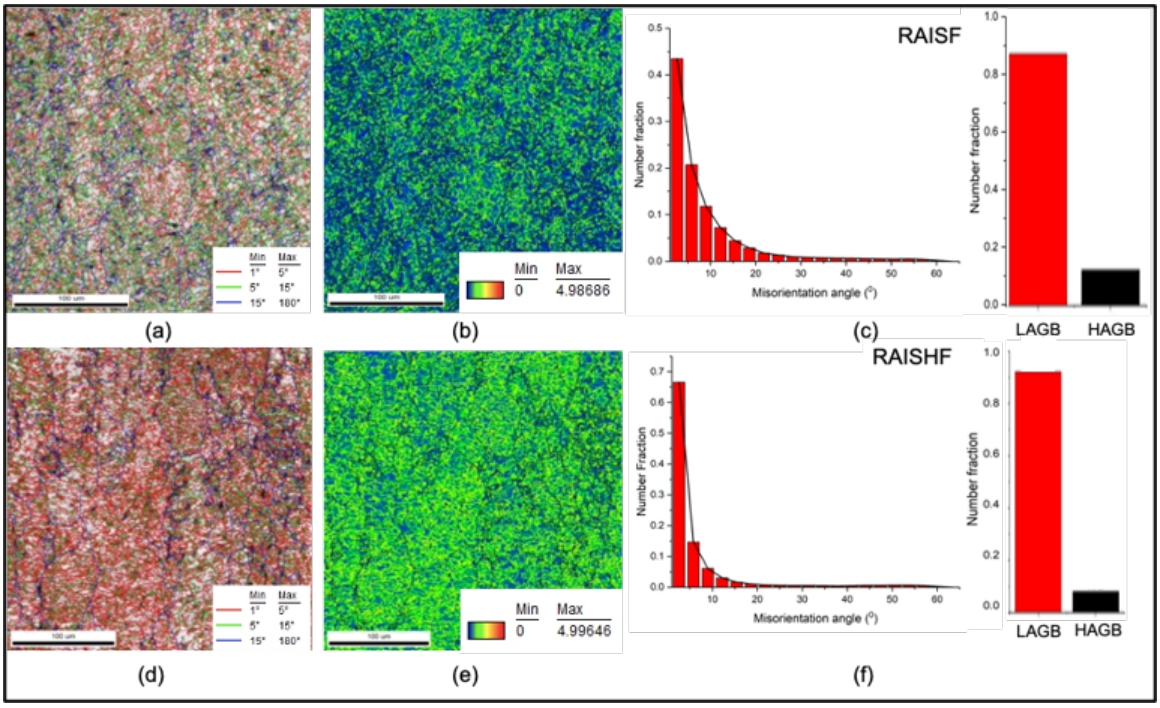

Figure 17: (a) Grain boundary map of RAISF sample, (b) KAM map of RAISF sample, (c) distribution of misorientation angle in the RAISF sample, (d) grain boundary map of RAISHF sample, (e) KAM map of RAISHF sample, and (f) distribution of misorientation angle in the RAISHF sample.

straight groove test and the following conclusions are drawn.

- More forming depth and lesser spring back was found in the cones fabricated by RAISHF than by RAISF.
- It has been revealed from FLC of RAISHF and RAISF that FLD for RAISHF is found to be raised due to larger formability of the sheet in that process. More in-plane strain was obtained in case of RAISHF than in RAISF.
- Due to hydrostatic nature of fluid pressure from back, more uniform thickness distribution is observed in case of RAISHF than that of RAISF.
- The micro hardness of the samples has been measured and is found that the sample in the middle region is hardest for the AA6061. Microhardness in case of RAISF is found to be higher than that in RAISHF.
- EBSD analysis has been carried out for studying the microstructural evolution in the undeformed sheet and formed by RAISF & RAISHF. It has been observed that significant grain refinement occurred from RAISF and RAISHF. Finer grains are found to be present in case of RAISF than in RAISHF.

Acknowledgement
The authors are grateful to DST-SERB for sponsoring the work through project MMER/2014/0068 titled 'Design, Development and Fabrication of an Incremental sheet hydroforming machine setup'.

Data Availability statement
The raw/processed data required to reproduce these findings cannot be shared at this time as the data also forms part of an ongoing study.

Consent for publication
Consent for publication was obtained from all participants.

Conflict of interest
The authors declare that they have no conflict of interest

References

[1] EDWARD LESZAK. Apparatus and process for incremental dieless forming. URL `https://lens.org/177-750-492-332-96X`.

[2] WC Emmens, Gerd Sebastiani, and Antonius H van den Boogaard. The technology of incremental sheet forming—a brief review of the history. *Journal of Materials processing technology*, 210(8):981–997, 2010.

[3] WC Emmens and Antonius H van den Boogaard. An overview of stabilizing deform-

ation mechanisms in incremental sheet forming. *Journal of Materials Processing Technology*, 209(8):3688–3695, 2009.

[4] Shakir Gatea, Hengan Ou, and Graham McCartney. Review on the influence of process parameters in incremental sheet forming. *The International Journal of Advanced Manufacturing Technology*, 87:479–499, 2016.

[5] YH Kim and JJ Park. Effect of process parameters on formability in incremental forming of sheet metal. *Journal of materials processing technology*, 130:42–46, 2002.

[6] Myoung-Sup Shim and Jong-Jin Park. The formability of aluminum sheet in incremental forming. *Journal of Materials Processing Technology*, 113(1-3):654–658, 2001.

[7] Young-Kyun Kim, Soon-Hong Park, Ji-Hun Yu, Bandar AlMangour, and Kee-Ahn Lee. Improvement in the high-temperature creep properties via heat treatment of ti-6al-4v alloy manufactured by selective laser melting. *Materials Science and Engineering: A*, 715:33–40, 2018.

[8] SJ Yoon and Dong-Yol Yang. Investigation into a new incremental forming process using an adjustable punch set for the manufacture of a doubly curved sheet metal. *Proceedings of the Institution of Mechanical Engineers, Part B: Journal of Engineering Manufacture*, 215 (7):991–1004, 2001.

[9] Sahil Bharti, Eldho Paul, Anandu Uthaman, Hariharan Krishnaswamy, Alexandr Klimchik, and Riby Abraham Boby. Systematic analysis of geometric inaccuracy and its contributing factors in roboforming. *Scientific Reports*, 14 (1):20291, 2024.

[10] Swagatika Mohanty, Srinivasa Prakash Regalla, and YV Daseswara Rao. Robot-assisted incremental sheet metal forming under the different forming condition. *Journal of the Brazilian Society of Mechanical Sciences and Engineering*, 41:1–12, 2019.

[11] Swagatika Mohanty, Srinivasa Prakash Regalla, and YV Daseswara Rao. Effect of inclination and rotation of the sheet on sheet thinning and formability in robot assisted incremental sheet metal forming. *Materials Today: Proceedings*, 46:1039–1049, 2021.

[12] Swagatika Mohanty, Srinivasa Prakash Regalla, and Daseswara Rao YV. Investigation of influence of part inclination and rotation on surface quality in robot assisted incremental sheet metal forming (raisf). *CIRP Journal of Manufacturing Science and Technology*, 22:37–48, 2018.

[13] Guoqiang Fan, L Gao, G Hussain, and Zhaoli Wu. Electric hot incremental forming: A novel technique. *International Journal of Machine Tools and Manufacture*, 48(15):1688–1692, 2008.

[14] Amar Al-Obaidi, Verena Kräusel, and Dirk Landgrebe. Hot single-point incremental forming assisted by induction heating. *The International Journal of Advanced Manufacturing Technology*, 82:1163–1171, 2016.

[15] Swarit Anand Singh, Satwik Priyadarshi, and Puneet Tandon. Comparative study of incremental forming and elevated temperature incremental forming through experimental investigations on aa 1050 sheet. *Journal of Manufacturing Science and Engineering*, 143(6): 064501, 2021.

[16] San Zhang, GH Tang, Zhen Li, Xiangkui Jiang, and KeJie Li. Experimental investigation on the springback of az31b mg alloys in warm incremental sheet forming assisted with oil bath heating. *The International Journal of Advanced Manufacturing Technology*, 109:535–551, 2020.

[17] JR Duflou, Bart Callebaut, Johan Verbert, and Hans De Baerdemaeker. Laser assisted incremental forming: formability and accuracy improvement. *CIRP annals*, 56(1):273–276, 2007.

[18] Alexander Göttmann, Jö Diettrich, Georg Bergweiler, Markus Bambach, Gerhard Hirt, Peter Loosen, and Reinhart Poprawe. Laser-assisted asymmetric incremental sheet forming of titanium sheet metal parts. *Production Engineering*, 5:263–271, 2011.

[19] Saeid Amini, Ahmad Hosseinpour Gollo, and Hossein Paktinat. An investigation of conventional and ultrasonic-assisted incremental forming of annealed aa1050 sheet. *The International Journal of Advanced Manufacturing Technology*, 90:1569–1578, 2017.

[20] Yanle Li, Xiaoxiao Chen, Jie Sun, Jianfeng Li, and Guoqun Zhao. Effects of ultrasonic vibration on deformation mechanism of incremental point-forming process. *Procedia Engineering*, 207:777–782, 2017.

[21] Horst Meier, B Buff, and V Smukala. Robot-based incremental sheet metal forming–increasing the part accuracy in an automated,

industrial forming cell. *Key Engineering Materials*, 410:159–166, 2009.

[22] Balaji Ilangovan. *Fixtureless automated incremental sheet metal forming*. PhD thesis, Loughborough University, 2016.

[23] Lars Thyssen, Christian Simon Magnus, Denis Daniel Störkle, and Bernd Kuhlenkötter. Compensating geometric inaccuracies in incremental sheet forming at elevated temperatures. *Procedia engineering*, 207: 860–865, 2017.

[24] Gerhard Hirt, Roman Kordtomeikel, Thomas Bremen, Marvin Laugwitz, and David Bailly. On the geometrical accuracy in incremental sheet forming. In *Forming the Future: Proceedings of the 13th International Conference on the Technology of Plasticity*, pages 507–521. Springer, 2021.

[25] Huaqing Ren, Jiaxi Xie, Shuheng Liao, Dohyun Leem, Kornel Ehmann, and Jian Cao. In-situ springback compensation in incremental sheet forming. *CIRP Annals*, 68(1): 317–320, 2019.

[26] Abdul Qadeer, G Hussain, Mohammed Alkahtani, and Johannes Buhl. Springback behavior of a metal/polymer laminate in incremental sheet forming: stress/strain relaxation perspective. *Journal of Materials Research and Technology*, 23:1725–1737, 2023.

[27] Paolo Bosetti and Stefania Bruschi. Springback evaluation of parts made by single-point incremental sheet forming. In *ASME International Mechanical Engineering Congress and Exposition*, volume 54891, pages 925–932, 2011.

[28] Haibo Lu, Michael Kearney, Chenhao Wang, Sheng Liu, and Paul A Meehan. Part accuracy improvement in two point incremental forming with a partial die using a model predictive control algorithm. *Precision Engineering*, 49: 179–188, 2017.

[29] Jae-Hyeong Yu, Kyu-Seok Jung, Mohanraj Murugesan, Wan-Jin Chung, and Chang-Whan Lee. Study on the incremental sheet metal forming process using a metal foam as a die. *International Journal of Material Forming*, 15(6):71, 2022.

[30] Hiroki Ichihara and Akio Sekiguchi. Development of elastomer-based incremental sheet forming method for curved products. *Procedia Manufacturing*, 15:1184–1191, 2018.

[31] K McLoughlin, A Cognot, and E Quigley. Dieless manufacturing of sheet metal components with non rigid support. *Proc. SheMet 2003*, pages 123–130, 2003.

[32] Noomane Ben Khalifa and Sebastian Thiery. Incremental sheet forming with active medium. *CIRP Annals*, 68(1):313–316, 2019.

[33] S Thiery and N Ben Khalifa. Geometrical accuracy in two-stage incremental sheet forming with active medium. In *Production at the Leading Edge of Technology: Proceedings of the 11th Congress of the German Academic Association for Production Technology (WGP), Dresden, September 2021*, pages 65–74. Springer, 2022.

[34] Yao Zimeng, Liang Xiaoming, Wu Shenli, Liu Ling, and Bai Lang. Effect of isostatic pressing support on forming force in single point incremental forming. *Integrated Ferroelectrics*, 236 (1):150–163, 2023.

[35] Miao Shang, Yan Li, Kuangyu Chen, Mingshun Yang, Xingbai Zhao, and Kaixin Nie. Incremental forming of hydraulic supports: a numerical and experimental study of thickness distribution. *Journal of Mechanical Science and Technology*, 37(12):6477–6491, 2023.

[36] Miao Shang, Yan Li, Mingshun Yang, Yunshuai Chen, Lang Bai, and Pengyang Li. Wall thickness uniformity in isf of hydraulic support: system design, finite element analysis and experimental verification. *Machines*, 11 (3):353, 2023.

[37] YOGESH Kumar and SANTOSH Kumar. Analysis of incremental sheet forming process through simulation. *Int. J. Mech. Prod. Eng. Res. Dev*, 8(3):145–152, 2018.

[38] Yogesh Kumar and Santosh Kumar. Experimental and analytical evaluation of incremental sheet hydro-forming strategies to produce high forming angle sheets. *Heliyon*, 5(6), 2019.

[39] Ravi Prakash Singh, Santosh Kumar, Pankaj Kumar Singh, and Md Meraz. Experimental investigation of multi-stage robot-assisted single point incremental sheet forming of al 6061 sheet. In *Advances in Forming, Machining and Automation: Select Proceedings of AIMTDR 2021*, pages 61–69. Springer, 2022.

[40] Santosh Kumar and Yogesh Kumar. Robot assisted high speed incremental sheet hydroforming machine.

[41] Ravi Prakash Singh, Santosh Kumar, Pankaj Kumar Singh, Md Meraz, and Sachin Salunkhe. Advancements in robot-assisted incremental sheet hydroforming: a comparative analysis of formability, mechanical properties, and surface finish for rhomboidal and conical frustums. *International Journal of Intelligent Robotics and Applications*, pages 1–13, 2024.

[42] Ravi Prakash Singh, Sandeep Kumar Gupta, Pankaj Kumar Singh, and Santosh Kumar. Robot assisted incremental sheet forming of al6061 under static pressure: Preliminary study of thickness distribution within the deformation region. *Materials Today: Proceedings*, 47:2737–2741, 2021.

[43] RP Singh, Santosh Kumar, EJ Brambley, Sisir Dhara, and Pankaj Kumar Singh. A simplified approach for formability optimization on incremental sheet forming using straight groove test and vwacf. manuscript under communication.

[44] Aditya H Naronikar, HN Akshay Jamadagni, Amruthamshu Simha, and B Saikiran. Optimizing the heat treatment parameters of al-6061 required for better formability. *Materials Today: Proceedings*, 5(11):24240–24247, 2018.

[45] D Banabic, L Lazarescu, L Paraianu, I Ciobanu, I Nicodim, and DS Comsa. Development of a new procedure for the experimental determination of the forming limit curves. *CIRP Annals*, 62(1):255–258, 2013.

[46] Scott Taylor, Iain Masters, Zushu Li, and Hiren R Kotadia. Comparison of formability and microstructural evolution of c106 copper and 316l stainless steel. *JOM*, 71:2721–2727, 2019.

[47] Michael A Sutton, Jean Jose Orteu, and Hubert Schreier. *Image correlation for shape, motion and deformation measurements: basic concepts, theory and applications*. Springer Science & Business Media, 2009.

[48] Sumit HAZRA, Sisir DHARA, Scott TAYLOR, and Łukasz FIGIEL. The non-proportional loading of mild steel. *Materials Research Proceedings*, 41, 2024.

[49] Ghulam Hussain, Nasir Hayat, and Gao Lin. Pyramid as test geometry to evaluate formability in incremental forming: Recent results. *Journal of mechanical science and technology*, 26:2337–2345, 2012.

[50] Yingbin Bao and Tomasz Wierzbicki. On fracture locus in the equivalent strain and stress triaxiality space. *International journal of mechanical sciences*, 46(1):81–98, 2004.

[51] Tomasz Wierzbicki, Yingbin Bao, Young-Woong Lee, and Yuanli Bai. Calibration and evaluation of seven fracture models. *International Journal of Mechanical Sciences*, 47(4-5): 719–743, 2005.

[52] Yanshan Lou, Hoon Huh, Sungjun Lim, and Keunhwan Pack. New ductile fracture criterion for prediction of fracture forming limit diagrams of sheet metals. *International Journal of Solids and Structures*, 49(25):3605–3615, 2012.

[53] Frank A McClintock. A criterion for ductile fracture by the growth of holes. *Journal of Applied Mechanics*, 35(2):363–371, 1968.

[54] J R_ Rice and Dennis Michael Tracey. On the ductile enlargement of voids in triaxial stress fields. *Journal of the Mechanics and Physics of Solids*, 17(3):201–217, 1969.

[55] Shakir Gatea, Hengan Ou, Bin Lu, and Graham McCartney. Modelling of ductile fracture in single point incremental forming using a modified gtn model. *Engineering Fracture Mechanics*, 186:59–79, 2017.

[56] IE French and PF Weinrich. The effects of hydrostatic pressure on the mechanism of tensile fracture of aluminum. *Metallurgical Transactions A*, 6:1165–1169, 1975.

[57] DS Liu, M Manoharan, and JJ Lewandowski. Effects of microstructure of the behavior of an aluminum alloy and an aluminum matrix composite tested under low levels of superimposed hydrostatic pressure. *Metallurgical Transactions A*, 20:2409–2417, 1989.

[58] Boaz Avitzur and Betzalel Avitzur. Pressure-induced ductility. *Journal of Manufacturing Science and Engineering*, 92:419–426, 1970.

[59] SP Keeler. Forming limit criteria—sheets. In *Advances in deformation processing*, pages 127–157. Springer, 1978.

[60] Fahrettin Ozturk, Murat Dilmec, Mevlut Turkoz, Remzi E Ece, and Huseyin S Halkaci. Grid marking and measurement methods for sheet metal formability. In *5th International Conference and Exhibition on Design and Production of MACHINES and DIES/MOLDS*, pages 18–21, 2009.

[61] Walter Lorrek and Oskar Pawelski. The influence of hydrostatic pressure on the plastic deformation of metallic materials. In *Proceedings of the Fifteenth International Machine Tool*

Design and Research Conference, pages 703–712. Springer, 1975.

[62] M Yajima, M Ishii, and M Kobayashi. The effects of hydrostatic pressure on the ductility of metals and alloys. *International Journal of Fracture Mechanics*, 6:139–150, 1970.

[63] Giuseppina Ambrogio, Luigino Filice, Francesco Gagliardi, and Fabrizio Micari. Sheet thinning prediction in single point incremental forming. *Advanced materials research*, 6:479–486, 2005.

[64] D Young and J Jeswiet. Wall thickness variations in single-point incremental forming. *Proceedings of the Institution of Mechanical Engineers, Part B: Journal of Engineering Manufacture*, 218(11):1453–1459, 2004.

[65] TJ Kim and Dong-Yol Yang. Improvement of formability for the incremental sheet metal forming process. *International Journal of Mechanical Sciences*, 42(7):1271–1286, 2000.

[66] Yuhyeong Jeong, Giseung Shin, Choo Woong, Jeoung Han Kim, and Jonghun Yoon. Dissimilar materials welding with a standoff-free vaporizing foil actuator between trip 1180 steel sheets and aa5052 alloy. *Materials*, 14(17): 4969, 2021.

[67] MB Silva, Martin Skjødt, Paulo AF Martins, and Niels Bay. Revisiting the fundamentals of single point incremental forming by means of membrane analysis. *International Journal of Machine Tools and Manufacture*, 48(1):73–83, 2008.

[68] Hao Wu and Guohua Fan. An overview of tailoring strain delocalization for strength-ductility synergy. *Progress in Materials Science*, 113:100675, 2020.

[69] ME Fitzpatrick, AT Fry, P Holdway, FA Kandil, J Shackleton, and L Suominen. Measurement good practice guide no. 52. *Determination of residual stresses by X-ray diffraction*, (2):1–68, 2005.

[70] Abhishek Kumar, HK Mehtani, Amber Shrivastava, Sushil Mishra, K Narasimhan, and Indradev Samajdar. Failure mechanism during incremental sheet forming of a commercial purity aluminum alloy. *Engineering Failure Analysis*, 146:107090, 2023.

[71] Jun-chao Li, Fen-fen Yang, and Zhi-qiang Zhou. Thickness distribution of multi-stage incremental forming with different forming stages and angle intervals. *Journal of Central South University*, 22(3):842–848, 2015.

[72] B Bay, N Hansen, and D Kuhlmann-Wilsdorf. Deformation structures in lightly rolled pure aluminium. *Materials Science and Engineering: A*, 113:385–397, 1989.

[73] Zhidong Chang, Mei Yang, and Jun Chen. Experimental investigations on deformation characteristics in microstructure level during incremental forming of aa5052 sheet. *Journal of Materials Processing Technology*, 291:117006, 2021.

[74] Abhishek Kumar, Amber Shrivastava, K Narasimhan, and Sushil Mishra. Microstructure and texture evolution during incremental sheet forming of aa1050 alloy. *Journal of Materials Science*, 57(11): 6385–6398, 2022.

[75] Karl G Schell, Fabian Lemke, Ethel C Bucharsky, A Hintennach, and MJ Hoffmann. Microstructure and mechanical properties of li 0.33 la 0.567 tio 3. *Journal of Materials Science*, 52:2232–2240, 2017.

[76] Qiuzhi Gao, Hailian Zhang, Huijun Li, Xin Zhang, Fu Qu, Yujiao Jiang, Ziyun Liu, and Chenchen Jiang. Hot deformation of alumina-forming austenitic steel: Ebsd study and flow behavior. *Journal of Materials Science*, 54 (11):8760–8777, 2019.

[77] Myrjam Winning and Anthony D Rollett. Transition between low and high angle grain boundaries. *Acta materialia*, 53(10):2901–2907, 2005.